EDGE ARTICLE

Entropy directs the self-assembly of supramolecular palladium coordination macrocycles and cages†

D. A. Poole III, E. O. Bobylev, S. Mathew and J. N. H. Reek [iD] *

The self-assembly of palladium-based cages is frequently rationalized *via* the cumulative enthalpy (ΔH) of bonds between coordination nodes (**M**, *i.e.*, Pd) and ligand (**L**) components. This focus on enthalpic rationale limits the complete understanding of the Gibbs free energy (ΔG) for self-assembly, as entropic (ΔS) contributions are overlooked. Here, we present a study of the $M_2^{lin}L_3$ intermediate species (**M** = dinitrato(N,N,N',N'-tetramethylethylenediamine)palladium(II), ^{lin}L = 4,4′-bipyridine), formed during the synthesis of triangle-shaped ($M_3^{lin}L_3$) and square-shaped ($M_4^{lin}L_4$) coordination macrocycles. Thermochemical analyses by variable temperature (VT) ^{1}H-NMR revealed that the $M_2^{lin}L_3$ intermediate exhibited an unfavorable (relative) ΔS compared to $M_3^{lin}L_3$ (triangle, $\Delta T \Delta S$ = +5.22 kcal mol^{-1}) or $M_4^{lin}L_4$ (square, $\Delta T \Delta S$ = +2.37 kcal mol^{-1}) macrocycles. Further analysis of these constructs with molecular dynamics (MD) identified that the self-assembly process is driven by ΔG losses facilitated by increases in solvation entropy (ΔS_{solv}, *i.e.*, depletion of solvent accessible surface area) that drives the self-assembly from "open" intermediates toward "closed" macrocyclic products. Expansion of our computational approach to the analysis of self-assembly in $Pd_n^{ben}L_{2n}$ cages (^{ben}L = 4,4'-(5-ethoxy-1,3-phenylene) dipyridine), demonstrated that ΔS_{solv} contributions drive the self-assembly of both thermodynamic cage products (*i.e.*, $Pd_{12}^{ben}L_{24}$) and kinetically-trapped intermediates (*i.e.*, $Pd_8^cL_{16}$).

Introduction

Self-assembled macrocycles,[1–7] cages,[8–13] and oligomers[14–16] featuring palladium-coordination nodes are a mainstay of supramolecular chemistry due to their unique mechanical,[14–18] optoelectronic,[19–28] and catalytic[29–42] applications. The square-planar coordination geometry of the coordination node permits the synthesis of well-defined constructs invoking simple geometric design principles.[43–48] These constructs are formed by the spontaneous self-assembly of palladium-based coordination nodes with ditopic ligands, affording highly-ordered assemblies bearing the minimum Gibbs free energy (ΔG).[43–50] The synthesis of these assemblies from their many constituent components is rationalized by the cumulative enthalpic (ΔH) contributions as a result of the formation of dative bonds between ditopic ligands and Pd-based coordination nodes.[49,50] However, studies of gas-phase reactivity reveal these ΔH contributions decrease with sequential coordination of additional ligands, favoring the formation of coordinatively

Homogeneous, Supramolecular, and Bioinspired Catalysis Group, van 't Hoff Institute for Molecular Science (HIMS), University of Amsterdam (UvA), Science Park 904, 1098 XH Amsterdam, The Netherlands. E-mail: j.n.h.reek@uva.nl

unsaturated oligomers.[51] In addition, currently only entropic contributions (ΔS) based on statistical arguments are taken into account, implying that assemblies based on a large number of components are entropically largely unfavorable despite many synthetic examples. Whereas similar enthalpic arguments rationalize the difference in energy between various assemblies, it remains unclear why well-defined structures are favored over oligomers as these coordination bonds in principle can be formed with limited constraints. The current rationale for deducing self-assembly thermodynamics is therefore incomplete, which motivates our current study.

The self-assembly of equimolar amounts of dinitrato(N,N,N',N'-tetramethylethylenediamine)palladium(II) (**M**) and 4,4′-bipyridine (^{lin}L) affords a mixture of triangular and square macrocycles in equilibrium (Scheme 1).[1,2]

Previous reports have leveraged this experimentally accessible equilibrium to measure the relative ΔS and ΔH of triangular and square complexes.[5] These studies found that ΔS favors the assembly featuring fewer components (*i.e.*, triangles) while ΔH favors the geometric matching between the square-planar metal center and the ligand geometry (*i.e.*, squares).[1,5] The synthesis of (and conversion between) macrocyclic assemblies proceeds *via* coordinatively unsaturated oligomeric intermediates (Scheme 1, purple).

Interestingly, similar stable oligomer intermediates have been found in the synthesis of polygonal organometallic
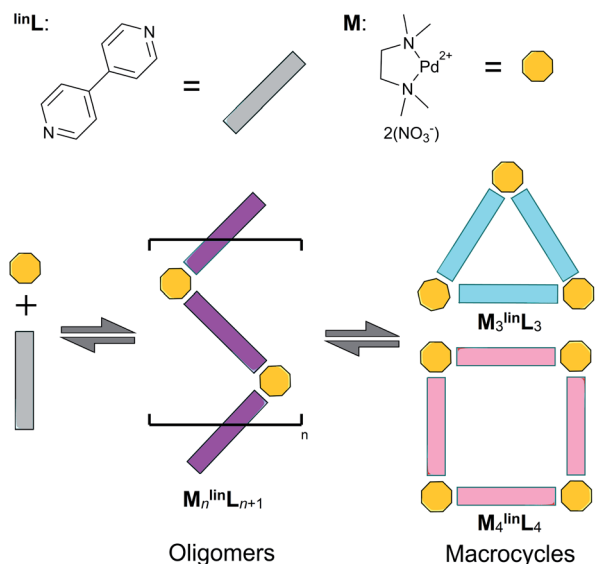
Scheme 1 Self-assembly of dinitrato(*N*,*N*,*N'*,*N'*-tetramethylethylene-diamine) palladium(II) (M, yellow) and 4'4-bipyridine (linL, grey) affording a mixture of triangular (M₃linL₃, blue) and square (M₄linL₄, pink) macrocycles alongside oligomer intermediates (MₙlinLₙ₊₁, purple).

Scheme 2 The self-assembly of Pd₁₂benL₂₄ cages (benL = 4,4'-(5-ethoxy-1,3-phenylene)dipyridine) *via* poorly defined reticular intermediates (green).

macrocyclic assemblies.[1–5] The equilibrium between these stable oligomeric intermediates and macrocyclic products may be leveraged to quantify ΔH and ΔS contributions to self-assembly using the literature described NMR-based approach.[5] Realization of the origin and effect of these thermodynamic contributions enables rational improvement of the self-assembly of highly-ordered constructs used broadly in supramolecular chemistry, including coordination cages, metal–organic frameworks, and dynamic-covalent based constructs.[52,59–62]

In this report, we demonstrate that the self-assembly of an equimolar mixture of **M** and **linL** in deuterated dimethyl sulfoxide (DMSO) affords a mixture of triangular (M₃linL₃) and square (M₄linL₄), and oligomeric (MₙlinLₙ₊₁) assemblies as depicted in Scheme 1.[1,6] We employed variable temperature ¹H-NMR (VT-NMR) to determine the ΔH and ΔS of both oligomeric and macrocyclic assemblies, providing unprecedented thermodynamic insights into the self-assembly process. Importantly, this thermodynamic data-enabled validation of a molecular dynamics (MD)[52] based approach to distinguish respective ΔS contributions arising from the assembly structure (ΔS_{struct}, eqn S1†)[53] and its solvation (ΔS_{solv}, eqn S2†).[54] These individual entropic contributions, alongside calculation of ΔH (eqn S3†), ultimately provide an accurate ΔG for self-assembly. We applied our MD-based approach to the study of coordination cages based on 4,4'-(5-ethoxy-1,3-phenylene)dipyridine as a bent ditopic ligand (benL) and free palladium(II) ions (Pd²⁺), which have been reported in the literature (Scheme 2).[8–13] Thermodynamic estimates derived from MD simulations reveal a ΔS_{solv}-driven, self-assembly process for macrocycles and cages reminiscent of biopolymer folding.[51] The generalization of our MD-based approach may distinguish between kinetically
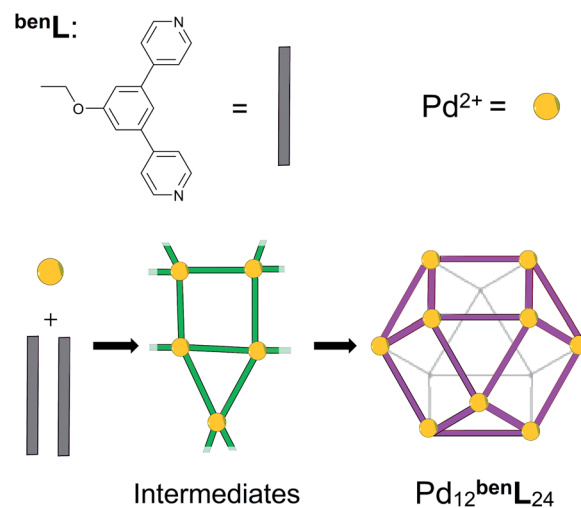
accessible thermodynamic products (*i.e.*, Pd₁₂benL₂₄) and undesirable kinetically-trapped intermediate assemblies (*e.g.* Pd₈benL₁₆).[55]

These computational and experimental studies demonstrate that ΔS drives the self-assembly of supramolecular constructs featuring palladium coordination nodes. As this ΔS contribution arises from solvation, these findings broadly reflect the thermodynamic drive of self-assembly to form compact supramolecular structures. Furthermore, we demonstrate the utility of MD-based approaches to quantify the thermodynamics of large supramolecular systems, providing a methodology that enables *in silico* studies of self-assembly processes.

Results

Synthesis and characterization of assemblies based on M and linL

Previously, we reported that the absence of trace halide impurities during the self-assembly of coordination cages resulted in slower formation kinetics, giving rise to the observation of intermediates.[49] Thus, we developed an alternative preparation for **M**, using a limiting quantity of palladium dichloride to minimize trace chloride (Scheme S1†). With this prepared metal precursor, the self-assembly of stoichiometric quantities of **M** and **linL** (M : linL = 1.0 : 1.0, [**M**] = 17.1 mM) affords a mixture of macrocyclic (M₃linL₃ and M₄linL₄) and oligomeric products evidenced by characteristic ¹H–NMR peaks shown in Fig. 1.

Peaks corresponding to M₃linL₃ (δ = 9.24 ppm) and M₄linL₄ (δ = 9.40 ppm) were consistent with the reported values of these macrocyclic species.[3] Two additional peaks (δ = 9.32–9.37 ppm) present, with chemical shifts consistent with reported oligomers,[1,2] and a single diffusion constant (D = 1.56 × 10⁻¹⁰ m² s⁻¹, Fig. 1 inset). These features indicate the presence of a single coordination assembly with a size larger than free linL (D = 1.86 × 10⁻¹⁰ m² s⁻¹) but smaller than M₃linL₃ (D = 1.20 × 10⁻¹⁰ m² s⁻¹). We also observed a near 2 : 1 ratio of α-pyridyl peak areas
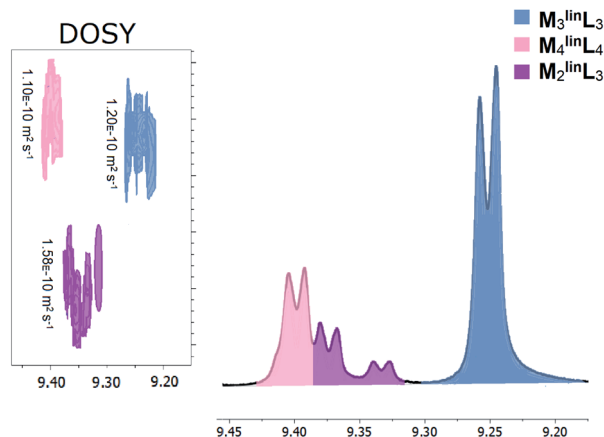
Fig. 1 Macrocyclic and oligomeric products observed from the self-assembly of M (17.1 mM) and ^{lin}L (17.1 mM) in DMSO characterized by unique α-pyridyl peaks in ^{1}H-NMR (Fig. S1†), with inset DOSY (Fig. S2†) diffusograms. Three distinct assemblies were observed and high-lighted for clarity: $M_3^{lin}L_3$ (slate blue), $M_4^{lin}L_4$ (pink), and $M_2^{lin}L_3$ (purple). Numerical data is provided below in Table 1.
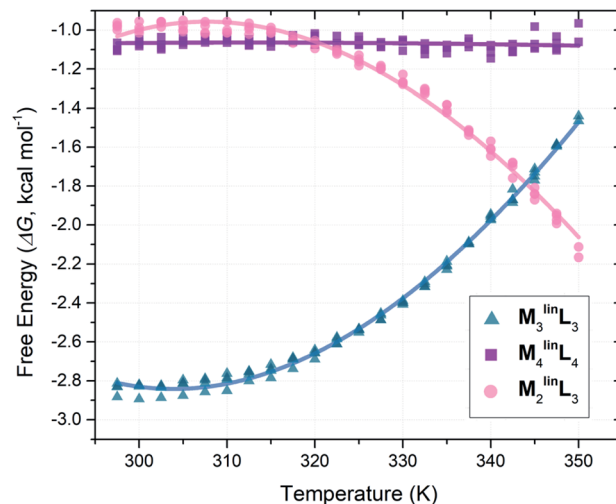

Fig. 2 Plot of ΔG versus temperature plot from VT-NMR measurements (^{1}H = 300 MHz, DMSO, T_r = 30 s) from quadruplicate temperature sweeps. Free energy values (ΔG) were computed from peak areas (Table 1) with a simplified reaction model (Scheme S2†).

Table 1 ^{1}H-NMR characterization of assemblies based on M and $^{lin}L^a$

Assembly	$\delta_{\alpha\text{-pyridyl}}$ (ppm)	$\delta_{\beta\text{-pyridyl}}$ (ppm)	% Area (α-pyridyl)	Diffusion, D ($\times 10^{-10}$ m^2 s^{-1})
$M_3^{lin}L_3$	9.24	8.28	63.9	1.20
$M_4^{lin}L_4$	9.40	8.21	21.2	1.10
$M_2^{lin}L_3^{\ b}$	9.37	8.24	9.9	1.58
$M_2^{lin}L_3^{\ c}$	9.32	8.19	5.0	1.58
$^{lin}L^{\ d}$	8.75	7.86	—	1.86

^{a} ^{1}H-NMR Conditions: DMSO, 300 K, 300 MHz. ^{b} Outer ligands, i.e., ^{lin}L-M-^{lin}L-M-^{lin}L. ^{c} Internal ligand, i.e., ^{lin}L-M-^{lin}L-M-^{lin}L. ^{d} Reference values were obtained separately for free ^{lin}L (Fig. S3).

(Table 1), assuming the overlap of α-pyridyl protons adjacent to coordination, we assigned these peaks to an oligomer species with the composition $M_2^{lin}L_3$.

While previous studies rationalized that the self-assembly process is driven to maximize the number of coordination bonds formed, affording coordinatively saturated species that minimize the ΔH of the system.[1] However, analysis by Weilandt et al. on mononuclear Pd complexes demonstrated that the formation of successive coordination bonds result in diminishing ΔH contributions to the ΔG of complex formation, which was partially compensated by ΔS.[56] Our observation of a significant presence of oligomeric (coordinatively unsaturated) assemblies (14.9%, Table 1), we infer that ΔS may play a similarly significant role in macrocycle assembly.

Thermochemical analysis of macrocycle–oligomer equilibria

Following the literature, we employed VT-NMR to quantify the relative abundance of assemblies ($M_2^{lin}L_3$, $M_3^{lin}L_3$, and $M_4^{lin}L_4$) by monitoring the intensity of their unique α-pyridyl peaks (Table 1) over a wide range of temperatures (297.5–350.0 K, see Fig. S12–S16†).[5] To determine the relative ΔG of $M_2^{lin}L_3$, $M_3^{lin}L_3$, and $M_4^{lin}L_4$ we modeled the system as three orthogonal

equilibria between each product and a common pool of reactants (Scheme S2†). These relative ΔG values (Table S1†) were plotted as a function of temperature (Fig. 2), and directly fit with an expanded van 't Hoff equation to compute ΔS and ΔH (Scheme S2†).[58]

Consistent with literature observations, these experimentally established ΔS and ΔH values confirm that $M_3^{lin}L_3$ and $M_4^{lin}L_4$ are the respective ΔS- and ΔH-favored macrocyclic products.[5] Interestingly, $M_2^{lin}L_3$ features a lower ΔH than the ΔH-favored $M_4^{lin}L_4$ (Table 2, ΔΔH = −2.27 kcal mol^{-1}) and an elevated −TΔS compared to the ΔS-favored $M_3^{lin}L_3$ (Table 2, ΔTΔS = +5.22 kcal mol^{-1}). These results are contrary to established geometric and component-number based rationale for ΔH- and ΔS-favored products.[1,4,5]

We surmise that the ΔH of $M_2^{lin}L_3$ derives from the conformational freedom of the structure, allowing the adoption of an unstrained configuration (∠N–Pd–N = 90°) following the geometric rationale established for $M_4^{lin}L_4$. However, $M_4^{lin}L_4$ exhibits an internal strain relative to $M_2^{lin}L_3$ manifesting as the ΔH-difference between the two complexes (ΔΔH = −2.27 kcal mol^{-1}). As both assemblies are presumed to adopt a conformation where ∠N–Pd–N = 90°, the apparent ΔΔH is

Table 2 Experimental thermodynamic differences between $M_2^{lin}L_3$, $M_3^{lin}L_3$, and $M_4^{lin}L_4$ coordination assemblies

Assembly	Relative thermodynamic parameters (kcal mol^{-1})^a		
	ΔH°	−TΔS°	ΔG°
$M_3^{lin}L_3$	0.00 ± 0.20	−2.80 ± 0.19	−2.80 ± 0.02
$M_4^{lin}L_4$	−1.11 ± 0.29	+0.05 ± 0.28	−1.06 ± 0.03
$M_2^{lin}L_3$	−3.38 ± 0.34	+2.42 ± 0.32	−0.96 ± 0.31

^{a} Values determined for T = 298.15 K by direct fitting a modified van 't Hoff model (Scheme S2) to VT-NMR derived ΔG values (Fig. 2).[58]

not accounted for when a simple geometric rationale is invoked.[1] Moreover, ΔS-differences between the 6-component $M_3{}^{lin}L_3$ and 5-component M_{2L3} contrast the typical rationale, which correlates the integration of fewer components to a favorable ΔS. These findings highlight how the current rationale for determining ΔS and ΔH contributions is insufficient to account for oligomeric assemblies, necessitating further computational investigation into the origins of internal strain found in $M_4{}^{lin}L_4$ and the unexpected ΔS penalties associated with $M_2{}^{lin}L_3$ formation.

MD analysis of experimental assemblies

Weilandt *et al.* suggested that two discrete ΔS factors that exert significant influence on metal–organic complex formation. The first is ΔS_{struct}, which decreases as more molecules (*i.e.*, components) are required to form a complex.[5] The other is ΔS_{solv}, which decreases as more solvent molecules are required to solvate a complex.[56] Using a previously described methodology,[52] we developed parameters to simulate assemblies comprised of M and ^{lin}L with accurate ΔH contributions (Fig. S4†). Using these parameters, and GBSA model solvation,[54] 50 ns trajectories (Fig. S5–S7†) were propagated by MD for $M_2{}^{lin}L_3$, $M_3{}^{lin}L_3$, and $M_4{}^{lin}L_4$ assemblies (Fig. 3). These trajectories were then used to compute the ΔS_{struct},[53] ΔS_{solv},[54] and ΔH contributions to ΔG (Table 3).

The thermodynamic contributions to ΔH and ΔS computed from these simulations (Table 3) differ those obtained by VT-NMR (Table 2) in their absolute value. However, the differences (*i.e.*, $\Delta\Delta G$, $\Delta\Delta H$, or $\Delta T\Delta S$) between assemblies measured by simulation and experiment are very similar (see below). The differences in absolute value reflect the different reference states in experimental and computational measurements (Fig. S20†). The reproduction of the relative differences in these physical quantities validates our *in silico* methodology for the thermodynamic values of these and similar assemblies.

The ΔH difference between $M_2{}^{lin}L_3$ and $M_4{}^{lin}L_4$ measured by VT-NMR ($\Delta\Delta H_{exp} = +2.28$ kcal mol^{-1}, Table 2), is similar to our MD-derived results ($\Delta\Delta H_{MD} = +2.20$ kcal mol^{-1}, Table 2). As ΔH generally originates from molecular geometry, we infer that the $M_4{}^{lin}L_4$ adopts a geometrically unfavorable (*i.e.*, strained) configuration compared to $M_2{}^{lin}L_3$. Visualization of MD trajectory data for $M_2{}^{lin}L_3$ assemblies reveals that this oligomer prefers a zig-zag conformation with a near-ideal square-planar coordination geometry at the Pd center ($\angle$N–Pd–N = 89°, Fig. 3c). In contrast, visualization of $M_4{}^{lin}L_4$ reveals a folded-square structure that features a hyperbolic geometry (*i.e.*, $\angle$N–Pd–N = 86°, Fig. 3b) giving rise to an internal strain that is enthalpically unfavorable (*i.e.*, elevates ΔH). Additional simulations of $M_4{}^{lin}L_4$ (performed *in vacuo*) reinforce that these distortions are a consequence of the solvation incurred to minimize the solvent-accessible surface area (Fig. S8†).

The $T\Delta S$ difference between $M_4{}^{lin}L_4$ and $M_2{}^{lin}L_3$ measured by VT-NMR ($\Delta T\Delta S_{exp} = +2.36$ kcal mol^{-1}, Table 2), is similar to our MD-derived results ($\Delta T\Delta S_{MD} = +2.37$ kcal mol^{-1}, Table 2), while other comparisons values have acceptable deviation (Fig. S20†). The calculated $-T\Delta S_{struct}$ values from our MD-approach
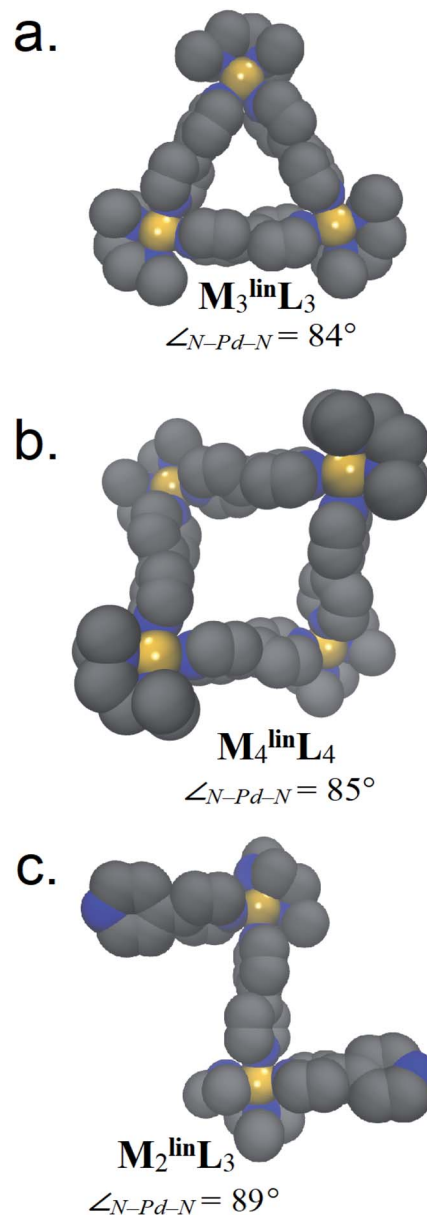
Fig. 3 Representative structures of (a) $M_3{}^{lin}L_3$, (b) $M_4{}^{lin}L_4$, and (c) $M_2{}^{lin}L_3$ are rendered with van der Waals representations of the non-hydrogen atoms. Relative thermodynamic contributions to ΔG are listed below in Table 3. Adjacent to each model is the average $\angle$N–Pd–N observed during MD.

Table 3 Thermodynamic values of assemblies based on M and ^{lin}L computed from MD trajectories

Assembly	Relative thermodynamic parameters (kcal mol^{-1})			
	$\Delta H°$	$-T\Delta S_{struct}°$	$-T\Delta S_{solv}°$	$\Delta G°$
$M_3{}^{lin}L_3$	+0.16	+4.15	−12.24	−7.93
$M_4{}^{lin}L_4$	−0.32	+6.15	−12.16	−6.33
$M_2{}^{lin}L_3$	−2.52	+1.30	−4.95	−6.17

decrease with the number of components (*i.e.*, $M_2{}^{lin}L_3$ < $M_3{}^{lin}L_3$ < $M_4{}^{lin}L_4$), in line with reported trends.[1,5] While, the computed difference of ΔS_{struct} for $M_3{}^{lin}L_3$ and $M_4{}^{lin}L_4$ are

similar to experimental values (Table 2), differences between both macrocycles *vs.* $M_2{}^{lin}L_3$ deviate significantly (Table 3). The inclusion of $-T\Delta S_{solv}$ improves the accounting for ΔS differences between $M_2{}^{lin}L_3$, $M_3{}^{lin}L_3$, and $M_4{}^{lin}L_4$ assemblies (Table 3). This leads us to infer that experimental $-T\Delta S$ penalties associated with $M_2{}^{lin}L_3$ formation originate from these ΔS_{solv} contributions, in agreement with thermodynamic studies of mono-nuclear Pd complexes.[56]

These thermodynamic parameters demonstrate that ΔS-specifically ΔS_{solv}-drives the conversion of oligomeric intermediates (*i.e.*, $M_2{}^{lin}L_3$) to their macrocyclic product assemblies (*i.e.*, $M_3{}^{lin}L_3$ and $M_4{}^{lin}L_4$). Moreover, the effect of ΔS_{solv} may overcome ΔH contributions, resulting in strained and distorted molecular geometries. While chemists have previously exploited ΔH to direct the formation of desired constructs, these findings reveal that ΔS ultimately drives the synthetic process of multi-component self-assembly.

MD modeling of arbitrary M_{nLn} and M_{nLn+1} assemblies

Oligomers similar to (and including) $M_2{}^{lin}L_3$ are theorized to form as intermediates in the self-assembly process of larger supramolecular structures (Scheme 1). Therefore, we utilized our MD-based approach to compare a range of oligomeric intermediates ($M_n{}^{lin}L_{n+1}$; $n = 1-28$) and the potential macrocyclic products ($M_n{}^{lin}L_n$; $n = 2-28$) to elucidate the role of individual thermodynamic parameters (ΔS_{solv}, ΔS_{struct}, and ΔH) on ΔG for the self-assembly of macrocycles (Fig. 4).

The resulting simulations reveal that both macrocyclic (Fig. 4a) and oligomeric (Fig. 4b) assemblies exhibit increasingly unfavorable ΔG with increasing assembly size driven by ΔS_{struct} contributions. The limited range of assemblies observed by NMR measurements (*i.e.*, $M_2{}^{lin}L_3$, $M_3{}^{lin}L_3$, and $M_4{}^{lin}L_4$) is rationalized by the elevated ΔG experienced for other possible structures. This outcome is consistent with ESI-HRMS analysis (Fig. S9†) that provides qualitative evidence for the existence of larger assemblies in low abundance (*i.e.*, low signal-to-noise).

The value of $-T\Delta S_{struct}$ increases with size (Fig. 4, blue trace) for the self-assembly of both oligomeric and macrocyclic products, consistent with the decreased degrees-of-freedom experienced upon aggregation.[57] Intriguingly, we find a nonlinear correlation between the size and ΔH of oligomeric assemblies that is absent for macrocyclic congeners. Visualization of MD trajectory data reveals that larger oligomer assemblies adopt a compact conformation (Fig. S10†), resulting in increased strain (*i.e.*, ΔH penalty) on the palladium–pyridyl bonds compared to the zig-zag conformation found in smaller assemblies such as $M_2{}^{lin}L_3$ (Fig. 3c). We infer that these compact suprastructures are necessary to realize a more compact assembly, akin to the folded structure observed for $M_4{}^{lin}L_4$ macrocycles (Fig. 3b). This trade-off between $-T\Delta S_{solv}$ and ΔH originates from solvation and distinguishes oligomeric assemblies from macrocyclic ones. As $-T\Delta S_{solv}$ favors the formation of compact suprastructures, it is reasonable to deduce that the self-assembly of product macrocycles, in general, is driven by ΔS_{solv} contributions.
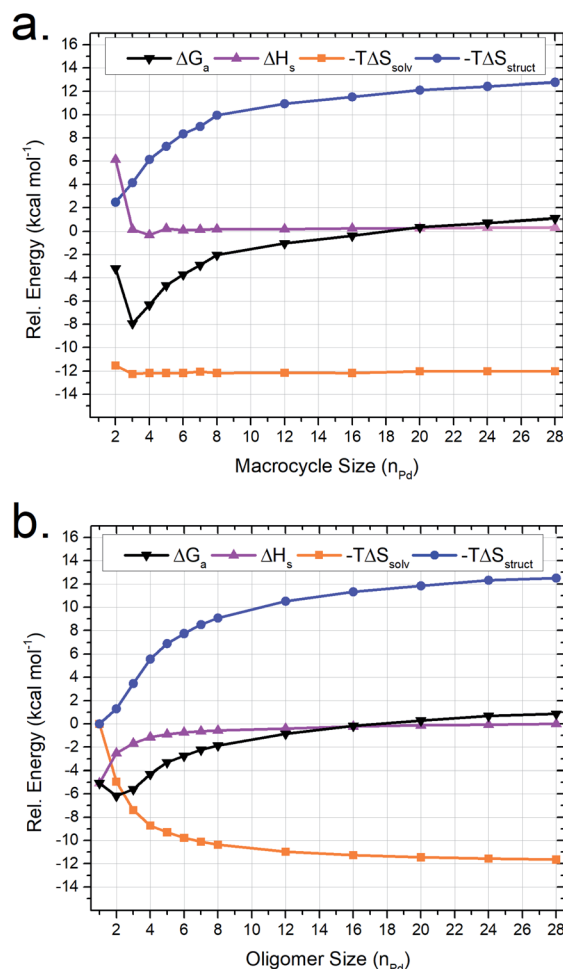

Fig. 4 MD-calculated thermodynamic parameters for (a) $M_n{}^{lin}L_n$ macrocyclic and (b) $M_n{}^{lin}L_{n+1}$ oligomeric assemblies. Energy values are plotted on a common scale where $-T\Delta S_{solv}$ and $-T\Delta S_{struct}$ contributions are plotted relative to $M_1{}^{lin}L_2$ while ΔH is plotted relative to $M_{28}{}^{lin}L_{29}$. The sum of $-T\Delta S_{solv}$, $-T\Delta S_{struct}$ and ΔH values is plotted as ΔG.

MD modeling of reticular cage self-assembly

Mixtures of bent ditopic ligands (^{ben}L = 4,4'-(5-ethoxy-1,3-phenylene)dipyridine) and free palladium(II) coordination nodes (Pd) self-assemble to afford cuboctahedral cages (Pd_{12}-$^{ben}L_{24}$) *via* oligomeric-assembly intermediates. We employed our MD-based approach to gain insight into the self-assembly process,[52] as incomplete or partial cages (*i.e.*, intermediate assemblies) are currently inaccessible by experimental methods (*e.g.*, CSI-HRMS, ¹H-NMR).[51] We developed models for intermediates of self-assembly ($Pd_n{}^{ben}L_m$, where $2n \le m \le 3n + 1$) from contiguous sections extracted from $Pd_{12}{}^{ben}L_{24}$, $Pd_8{}^{ben}L_{16}$, and $Pd_{15}{}^{ben}L_{30}$ cages, as well as a polymeric state ($Pd_n{}^{ben}L_m$, where $m = 3n + 1$) geometries. Then we elucidated the self-assembly pathway for these partially-formed constructs from their respective ΔS, ΔH, and ΔG values from MD-simulation (Fig. 5).

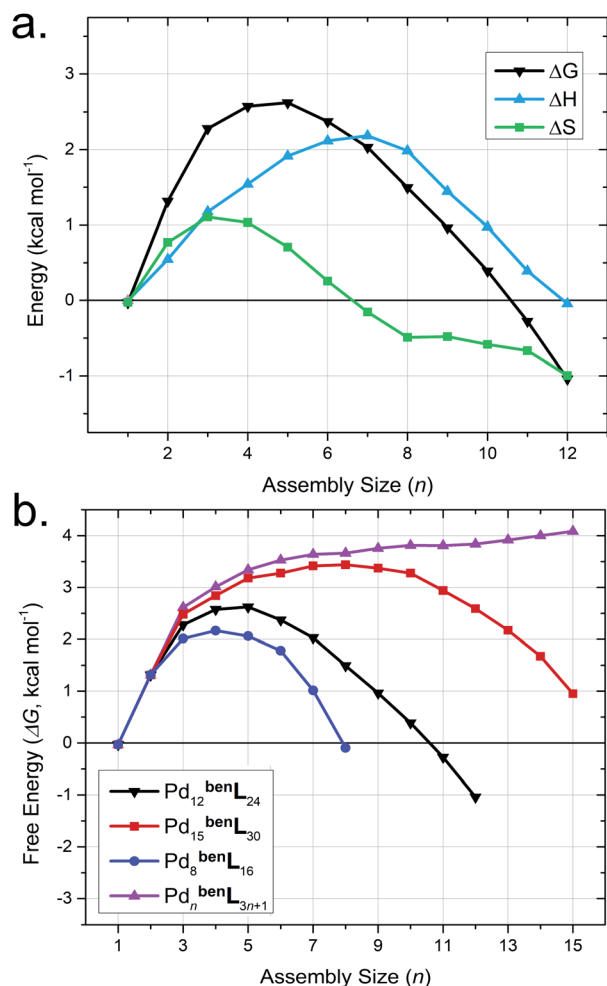Our simulations reveal the $Pd_{12}{}^{ben}L_{24}$ exhibits a lower ΔH (*i.e.*, minimal geometric strain) compared to congeneric

Fig. 5 MD-calculated thermodynamic parameters for the $Pd_n{}^{ben}L_m$ reticular intermediates ($2n \leq m \leq 3n$) for the self-assembly of Pd_{12}-$^{ben}L_{24}$ cages (a), alongside a comparison of the ΔG for $Pd_n{}^{ben}L_m$ reticular intermediates ($2n \leq m \leq 3n + 1$) for the self-assembly of $Pd_{12}{}^{ben}L_{24}$, $Pd_{15}{}^{ben}L_{30}$, $Pd_8{}^{ben}L_{16}$ cages and $Pd_n{}^{ben}L_{3n+1}$ polymers (b). Computed thermodynamic parameters values are presented relative to the $Pd_1{}^{ben}L_4$ complexes.

Table 4 MD-trajectory derived thermodynamic parameters of Pd_n-$^{ben}L_{2n}$ cages and $Pd_n{}^{ben}L_{3n+1}$ polymers

Assembly	Thermodynamic parameters (kcal mol^{-1})[a]			
	$\Delta H°$	$-T\Delta S_{struct}°$	$-T\Delta S_{solv}°$	$\Delta G°$
$Pd_8{}^{ben}L_{16}$	+1.20	+6.58	−7.88	−0.10
$Pd_{12}{}^{ben}L_{24}$	−0.04	+6.90	−7.90	−1.04
$Pd_{15}{}^{ben}L_{30}$	+1.70	+7.02	−7.77	+0.95
$Pd_{15}{}^{ben}L_{46}{}^{b}$	+1.60	+5.89	−3.41	+4.08

[a] Thermodynamic values are relative to those computed for $Pd_1{}^{ben}L_4$ assemblies. [b] Linear polymer assembly with the composition $Pd_n{}^{ben}L_{3n+1}$.

assemblies (Table 4). This observation is consistent with the literature and originates from the decreased metal–ligand bond strain experienced by this particular assembly-configuration.[8–13,49,52] Models of partially-formed assemblies (e.g.,

$Pd_5{}^{ben}L_{14}$) bear an elevated ΔH (Fig. 5a, blue trace) as a result of strain originating from deflation or collapse during MD simulations (Fig. S11†). Parallel observations have been made in $M_4{}^{lin}L_4$ macrocycles (Table 2), inferring increases in strain can act to offset penalties from solvation entropy (i.e., ΔS_{solv}), which leads to an overall elevation in ΔH for the system. The sum of entropic contributions (i.e., $\Delta S_{struct} + \Delta S_{solv} = \Delta S$, Fig. 5a, green trace) suggests that the formation of early intermediates ($n < 7$) is hindered while the self-assembly of spherical cages ($n = 12$) is encouraged. These results demonstrate that while ΔH directs the polyhedral geometry of the final assembly,[52,55] ΔS drives the structure of self-assembly to be spherical.

The comparison of the free energy (ΔG) pathways for the self-assembly of different topologies (Fig. 5b) enables us to distinguish between the thermodynamic product (i.e., $Pd_{12}{}^{ben}L_{24}$), kinetic traps (e.g., $Pd_8{}^{ben}L_{16}$),[55] and unrealized topologies (e.g., $Pd_{15}{}^{ben}L_{30}$, red trace). The maximum ΔG of intermediate assemblies of the $Pd_{15}{}^{ben}L_{30}$ pathway ($\Delta G_{max} = +3.44$ kcal mol^{-1}) is greater than that of the $Pd_{12}{}^{ben}L_{24}$ cage ($\Delta G_{max} = +2.62$ kcal mol^{-1}), rationalizing the possibility that intermediates may spontaneously reconfigure towards the latter structure as it is thermodynamically favored. In contrast, the $Pd_8{}^{ben}L_{16}$ pathway features the lowest maximum energy ($\Delta G_{max} = +2.17$ kcal mol^{-1}) of analyzed pathways demonstrating that kinetic traps are readily identified by our MD-based approach.

Conclusion

The thermochemical analysis of the self-assembly processes in palladium-based coordination macrocycles revealed unexpected ΔS-contributions that drive the formation of higher-order macrocycle assemblies ($M_3{}^{lin}L_3$ and $M_4{}^{lin}L_4$) from oligomer intermediates ($M_2{}^{lin}L_3$). Using an MD-based approach, we found that the driving force for self-assembly originates from the solvation entropy (i.e., ΔS_{solv}) of oligomeric intermediates that effects surface-area minimization of the construct. Thermodynamic trends were established by MD analysis of larger assemblies, revealing that both ΔS_{solv} and ΔS_{struct} direct the formation of assemblies that exhibit similar ΔH. Data from MD models of formation pathways for palladium-based coordination cages reveal that ΔS_{solv} is responsible for driving the self-assembly process. Further application of our MD approach enables rationalization of the formation $Pd_{12}{}^{ben}L_{24}$ cage products over kinetically trapped congeners (i.e., $Pd_8{}^{ben}L_{16}$) directly from the computed thermodynamic quantities (ΔS_{solv}, $\Delta S_{struct,}$ and ΔH) of the intermediate assemblies. Overall, these complementary experimental and computational investigations expose ΔS as the driver for the formation of these desirable highly ordered structures that have broad applications across supramolecular chemistry.

Author contributions

DAP conceived, designed and performed the experiments. EOB contributed ligand materials, performed HR-MS analyses and provided experimental expertise for self-assembly experiments. JNHR and SM supervised the work. DAP, SM, and JNHR wrote

the manuscript with all authors providing significant contributions to the analysis and interpretation of the work.

Conflicts of interest

There are no conflicts to declare.

Acknowledgements

Notes and references

1 M. Fujita, J. Yazaki and J. Ogura, *J. Am. Chem. Soc.*, 1990, **112**(14), 5645–5647, DOI: **10.1021/ja00170a042**.

2 M. Ferrer, A. Pedrosa, L. Rodríguez, O. Rossell and M. Vilaseca, *Inorg. Chem.*, 2010, **49**(20), 9438–9449, DOI: **10.1021/ic101150p**.

3 K. Uehara, K. Kasai and N. Mizuno, *Inorg. Chem.*, 2010, **49**(4), 2008–2015, DOI: **10.1021/ic100011a**.

4 P. J. Stang, D. H. Cao, S. Saito and A. M. Arif, *J. Am. Chem. Soc.*, 1995, **117**(23), 6273–6283, DOI: **10.1021/ja00128a015**.

5 T. Weilandt, R. W. Troff, H. Saxell, K. Rissanen and C. A. Schalley, *Inorg. Chem.*, 2008, **47**(17), 7588–7598, DOI: **10.1021/ic800334k**.

6 M. Fujita, O. Sasaki, T. Mitsuhashi, T. Fujita, J. Yazaki, K. Yamaguchi and K. Ogura, *Chem. Commun.*, 1996, **13**, 1535, DOI: **10.1039/cc9960001535**.

7 M. Fujita, M. Tominaga, A. Hori and B. Therrien, *Acc. Chem. Res.*, 2005, **38**(4), 369–378, DOI: **10.1021/ar040153h**.

8 K. Harris, D. Fujita and M. Fujita, *Chem. Commun.*, 2013, **49**(60), 6703, DOI: **10.1039/c3cc43191f**.

9 S. R. Seidel and P. J. Stang, *Acc. Chem. Res.*, 2002, **35**(11), 972–983, DOI: **10.1021/ar010142d**.

10 E. Raee, Y. Yang and T. Liu, *Giant*, 2021, **5**, 100050, DOI: **10.1016/j.giant.2021.100050**.

11 R. A. S. Vasdev, D. Preston and J. D. Crowley, *Chem.–Asian J.*, 2017, **12**(19), 2513–2523, DOI: **10.1002/asia.201700948**.

12 T. K. Ronson, S. Zarra, S. P. Black and J. R. Nitschke, *Chem. Commun.*, 2013, **49**(25), 2476, DOI: **10.1039/c2cc36363a**.

13 S. J. Dalgarno, N. P. Power and J. L. Atwood, *Coord. Chem. Rev.*, 2008, **252**(8–9), 825–841, DOI: **10.1016/j.ccr.2007.10.010**.

14 E. C. Constable, K. Harris, C. E. Housecroft and M. Neuburger, *Dalton Trans.*, 2011, **40**(7), 1524, DOI: **10.1039/c0dt01216e**.

15 D. Xu and S. L. Craig, *Macromolecules*, 2011, **44**(18), 7478–7488, DOI: **10.1021/ma201386t**.

16 D. Xu and S. L. Craig, *J. Phys. Chem. Lett.*, 2010, **1**(11), 1683–1686, DOI: **10.1021/jz1004818**.

17 A. V. Zhukhovitskiy, M. Zhong, E. G. Keeler, V. K. Michaelis, J. E. P. Sun, M. J. A. Hore, D. J. Pochan, R. G. Griffin, A. P. Willard and J. A. Johnson, *Nat. Chem.*, 2015, **8**(1), 33–41, DOI: **10.1038/nchem.2390**.

18 S. Krishnaswamy, S. Prusty, D. Chartrand, G. S. Hanan and D. K. Chand, *Cryst. Growth Des.*, 2018, **18**(4), 2016–2030, DOI: **10.1021/acs.cgd.7b01425**.

19 P. J. Stang and D. H. Cao, *J. Am. Chem. Soc.*, 1994, **116**(11), 4981–4982, DOI: **10.1021/ja00090a051**.

20 Q. Zhang, D. Tang, J. Zhang, R. Ni, L. Xu, T. He, X. Lin, X. Li, H. Qiu, S. Yin and P. J. Stang, *J. Am. Chem. Soc.*, 2019, **141**(44), 17909–17917, DOI: **10.1021/jacs.9b09671**.

21 J.-H. Tang, Y. Li, Q. Wu, Z. Wang, S. Hou, K. Tang, Y. Sun, H. Wang, H. Wang, C. Lu, X. Wang, X. Li, D. Wang, J. Yao, C. J. Lambert, N. Tao, Y.-W. Zhong and P. J. Stang, *Nat. Commun.*, 2019, **10**(1), 4599, DOI: **10.1038/s41467-019-12534-6**.

22 K. Acharyya, S. Bhattacharyya, H. Sepehrpour, S. Chakraborty, S. Lu, B. Shi, X. Li, P. S. Muckherjee and P. J. Stang, *J. Am. Chem. Soc.*, 2019, **141**(37), 14565–14569, DOI: **10.1021/jacs.9b08403**.

23 H. Zhu, Q. Li, B. Shi, H. Xing, Y. Sun, S. Lu, L. Shangguan, X. Li, F. Huang and P. J. Stang, *J. Am. Chem. Soc.*, 2020, **142**(41), 17340–17345, DOI: **10.1021/jacs.0c09598**.

24 W. Tuo, Y. Sun, S. Lu, X. Li, Y. Sun and P. J. Stang, *J. Am. Chem. Soc.*, 2020, **142**(40), 16930–16934, DOI: **10.1021/jacs.0c08697**.

25 Z. Yang, Y. Wang, X. Liu, R. T. Vanderlinden, R. Ni, X. Li and P. J. Stang, *J. Am. Chem. Soc.*, 2020, **142**(32), 13689–13964, DOI: **10.1021/jacs.0c06666**.

26 Y.-Q. He, W. Fudickar, J.-H. Tang, H. Wang, X. Li, J. Han, Z. Wang, M. Liu, Y.-W. Zhong, T. Linker and P. J. Stang, *J. Am. Chem. Soc.*, 2020, **142**(5), 2601–2608, DOI: **10.1021/jacs.9b12693**.

27 C. Chen, Y. Sun, Y. Zhao, R. T. van der Linden, W. Tuo, F. Zhang, S. Zhang, H. Sepehrpour, C. Yan, J. Wang, D. Li and P. J. Stang, *Proc. Natl. Acad. Sci. U. S. A.*, 2021, **118**, DOI: **10.1073/pnas.2102602118**.

28 R. Zaffaroni, E. O. Bobylev, R. Plessius, J. I. van der Vlugt and J. N. H. Reek, *J. Am. Chem. Soc.*, 2020, **142**(19), 8837–8847, DOI: **10.1021/jacs.0c01869**.

29 Y. Ueda, H. Ito, D. Fujita and M. Fujita, *J. Am. Chem. Soc.*, 2017, **139**(17), 6090–6093, DOI: **10.1021/jacs.7b02745**.

30 B. Chen, J. J. Holstein, S. Horiuchi, W. G. Hiller and G. H. Clever, *J. Am. Chem. Soc.*, 2019, **141**, 8907–8913, DOI: **10.1021/jacs.9b02207**.

31 R. Zaffaroni, N. Orth, I. Ivanović-Burmazović and J. N. H. Reek, *Angew. Chem., Int. Ed.*, 2020, **59**(42), 18485–18489, DOI: **10.1002/anie.202008298**.

32 S. Gonell, X. Caumes, N. Orth, I. Ivanović-Burmazović and J. N. H. Reek, *Chem. Sci.*, 2019, **10**, 1316–1321, DOI: **10.1039/c8sc03767a**.

33 F. Yu, D. Poole, S. Mathew, N. Yan, J. Hessels, N. Orth, I. Ivanović-Burmazović and J. N. H. Reek, *Angew. Chem., Int. Ed.*, 2018, **57**(35), 11247–11251, DOI: **10.1002/anie.201805244**.

34 R. Gramage-Doria, J. Hessels, S. H. A. M. Leenders, O. Tröppner, M. Dürr, I. Ivanović-Burmazović and

J. N. H. Reek, *Angew. Chem., Int. Ed.*, 2014, **53**(49), 13380–13384, DOI: **10.1002/anie.201406415**.

35 Q.-Q. Wang, S. Gonell, S. H. A. M. Leenders, M. Dürr, I. Ivanović-Burmazović and J. N. H. Reek, *Nat. Chem.*, 2016, **8**(3), 225–230, DOI: **10.1038/nchem.2425**.

36 L. J. Jongkind, X. Caumes, A. P. T. Hartendorp and J. N. H. Reek, *Acc. Chem. Res.*, 2018, **51**(9), 2115–2128, DOI: **10.1021/acs.accounts.8b00345**.

37 M. Yoshizawa, J. K. Klosterman and M. Fujita, *Angew. Chem., Int. Ed.*, 2009, **48**(19), 3418–3438, DOI: **10.1002/anie.200805340**.

38 H. Takezawa, K. Shitozawa and M. Fujita, *Nat. Chem.*, 2020, **12**, 574–578, DOI: **10.1038/s41557-020-0455-y**.

39 M. Yoshizawa, *Science*, 2006, **312**(5771), 251–254, DOI: **10.1126/science.1124985**.

40 W. Wang, Y.-X. Wang and H.-B. Yang, *Chem. Soc. Rev.*, 2016, **45**(9), 2656–2693, DOI: **10.1039/c5cs00301f**.

41 S. Hasegawa, S. L. Meichsner, J. J. Holstein, A. Baksi, M. Kasanmascheff and G. H. Clever, *J. Am. Chem. Soc.*, 2021, **143**(26), 9718–9723, DOI: **10.1021/jacs.1c02860**.

42 S. Bivaud, S. Goeb, V. Croué, M. Allain, F. Pop and M. Sallé, *Beilstein J. Org. Chem.*, 2015, **11**, 966–971, DOI: **10.3762/bjoc.11.108**.

43 T. R. Cook, Y.-R. Zheng and P. J. Stang, *Chem. Rev.*, 2012, **113**(1), 734–777, DOI: **10.1021/cr3002824**.

44 R. Chakrabarty, P. S. Mukherjee and P. J. Stang, *Chem. Rev.*, 2011, **111**(11), 6810–6918, DOI: **10.1021/cr200077m**.

45 D. Fujita, Y. Ueda, S. Sato, H. Yokoyama, N. Mizuno, T. Kumasaka and M. Fujita, *Chem*, 2016, **1**(1), 91–101, DOI: **10.1016/j.chempr.2016.06.007**.

46 C. Liu, E. O. Bobylev, Y. Fu, D. A. Poole, K. Robeyns, C. Fustin, Y. Garcia, J. N. H. Reek and M. L. Singleton, *Chem. - Eur. J.*, 2020, **26**(52), 11960–11965, DOI: **10.1002/chem.202001399**.

47 M. Fujita, *Chem. Soc. Rev.*, 1998, **27**(6), 417, DOI: **10.1039/a827417z**.

48 A. Tarzia, J. E. M. Lewis and K. E. Jelfs, *Angew. Chem., Int. Ed.*, 2021, **60**(38), 20879–20887, DOI: **10.1002/anie.202106721**.

49 E. O. Bobylev, D. A. Poole III, B. de Bruin and J. N. H. Reek, *Chem. Sci.*, 2021, **12**(22), 7696–7705, DOI: **10.1039/d1sc01295a**.

50 S. Pullen, J. Tessarolo and G. H. Clever, *Chem. Sci.*, 2021, **12**(21), 7269–7293, DOI: **10.1039/d1sc01226f**.

51 S. Hiraoka, *Bull. Chem. Soc. Jpn.*, 2018, **91**(6), 957–978, DOI: **10.1246/bcsj.20180008**.

52 D. A. Poole III., E. O. Bobylev, S. Mathew and J. N. H. Reek, *Chem. Sci.*, 2020, **11**, 12350–12357, DOI: **10.1039/D0SC03992F**.

53 R. M. Levy, M. Karplus, J. Kushick and D. Perahia, *Macromolecules*, 1984, **17**(7), 1370–1374, DOI: **10.1021/ma00137a013**.

54 R. B. Hermann, *J. Phys. Chem.*, 1972, **76**(19), 2754–2759, DOI: **10.1021/j100663a023**.

55 D. Fujita, H. Yokoyama, Y. Ueda, S. Sato and M. Fujita, *Angew. Chem., Int. Ed.*, 2014, **54**(1), 155–158, DOI: **10.1002/anie.201409216**.

56 T. Weilandt, N. L. Löw, G. Schnakenburg, J. Daniels, M. Nieger, C. A. Schalley and A. Lützen, *Chem. - Eur. J.*, 2012, **18**(52), 16665–16676, DOI: **10.1002/chem.201202771**.

57 D. A. McQuarrie, *Statistical Thermodynamics*, 1st edn, Harper and Row, 1973.

58 C. G. Maier and K. K. Kelly, *J. Am. Chem. Soc.*, 1932, **54**(8), 3243–3246, DOI: **10.1021/ja01347a029**.

59 P. Skowronek, B. Warżajtis, U. Rychlewska and J. Gawrońska, *Chem. Commun.*, 2013, **49**, 2524–2526, DOI: **10.1039/C3CC39098E**.

60 A. J. Greenlee, C. I. Wendell, M. M. Cencer, S. D. Laffoon and J. S. Moore, *Trends Chem.*, 2020, **2**(12), 1043–1051, DOI: **10.1016/j.trechm.2020.09.005**.

61 A. Bennett, A. F. Cheetham and F.-X. Coudert, *Nat. Chem.*, 2017, **9**, 11–16, DOI: **10.1038/nchem.2691**.

62 S. Jansze and K. Severin, *J. Am. Chem. Soc.*, 2019, **141**(2), 815–819, DOI: **10.1021/jacs.8b12738**.